Surfaces and Interfaces 41 (2023) 103191

Contents lists available at ScienceDirect

Surfaces and Interfaces

journal homepage: www.sciencedirect.com/journal/surfaces-and-interfaces

Smoothing of fused silica with less damage by a hybrid plasma process combining isotropic etching and atom-migration

Shaoxiang Liang [a], Yi He [a], Pengbo Ding [a], Chunjin Wang [b], Liang Guo [a,*], Hui Deng [a,c,*]

[a] Department of Mechanical and Energy Engineering, Southern University of Science and Technology, Shenzhen, Guangdong 518055, PR China
[b] State Key Laboratory of Ultra-precision Machining Technology, Department of Industrial and Systems Engineering, The Hong Kong Polytechnic University, Hung Hom, Kowloon, Hong Kong, China
[c] Institute for Applied Optics and Precision Engineering, Southern University of Science and Technology, Shenzhen, Guangdong 518055, P.R. China.

ARTICLE INFO

Keywords:
Atomic and close-to-atomic scale manufacturing
Plasma etching
Atom migration
Sub-surface damage
Roughness

ABSTRACT

In order to effectively reduce the subsurface damage of fused silica optics and obtain an ultra-smooth surface at atomic scale, we proposed a hybrid manufacturing process based on inductively coupled plasma (ICP), which combined isotropic etching polishing (IEP) and atom-migration manufacturing (AMM). In the plasma-IEP process, a large number of isotropic etching pits with ultra-smooth inner surface formed, enlarged, overlapped and merged, resulting in a smooth surface. The continuous downward etching process was accompanied by the continuous removal of the subsurface damage layer. With optimized process parameters, plasma-IEP could efficiently generate a less damage surface of fused silica with a material removal rate of 0.8 μm/min, and reduce the *Sa* roughness from 97.1 nm to 31.3 nm. The surface roughness could be further reduced to less than 0.15 nm by plasma-AMM, which was a non-subtractive finishing approach. The result of laser induced damage threshold (LIDT) test showed that the fused silica surface after the IEP-AMM hybrid manufacturing could withstand higher laser fluence, which implied more effective applications of this technique in high-power laser systems. This study proposed and verified the hybrid plasma manufacturing process combining plasma-IEP and plasma-AMM, which provided an ultra-smooth surface with less damage manufacturing process for fused silica.

1. Introduction

Fused silica is widely used in many fields as optical elements because of its excellent physical, chemical, electrical and optical properties. For example, in high-power laser systems, it is often used to make focusing lenses, beam splitters, gratings, and protective plates [1–3]. In semiconductor lithography systems, it is commonly used as a deep ultraviolet lithography (DUVL) material for light focusing [4,5]. In the above applications, the surface quality of fused silica optical elements has a direct impact on their performance [6,7]. For the achievement of ultrafine surface quality, ultra-precision machining technologies are continuously developing for the achievement of better machining accuracy [8]. However, in the present stage of optical manufacturing, mechanical removal based on plastic deformation is still the mainstream technology, so it inevitably introduces surface and subsurface damage, such as surface scratches and subsurface micro-cracks [9,10]. Therefore, how to reduce the subsurface damage of fused silica optics while pursuing the surface roughness of atomic level is the focus of research in recent years.

In order to remove surface and subsurface damage of fused silica, we studied a manufacturing process based on isotropic etching polishing using plasma (plasma-IEP) [11]. Under optimized conditions, the maximum material removal rate (MRR) of plasma-IEP on fused silica surface reached 5.62 μm/min. As a chemical etching process in atmosphere, plasma-IEP did not introduce new damage. However, previous studies showed that the roughness of the quartz surface after plasma-IEP was still on the order of 10 nm, despite of its great reduction compared with the initial ground surface. This is because the isotropic etching profile generated by plasma etching cannot completely disappear. Therefore, it can only be used as a semi-finishing method.

At present, the ultra-smooth surface manufacturing of fused silica optical elements mainly adopted computer controlled optical surfacing (CCOS) technology [12] and a variety of derivative optical manufacturing techniques, such as magnetorheological finishing (MRF) [13] and ion beam finishing (IBF) [14]. The wide applications of these technologies greatly improved the surface manufacturing accuracy of fused silica optical elements [15]. However, from the perspective of the

* Corresponding authors.
E-mail addresses: guol3@sustech.edu.cn (L. Guo), dengh@sustech.edu.cn (H. Deng).

https://doi.org/10.1016/j.surfin.2023.103191
Received 27 December 2022; Received in revised form 30 June 2023; Accepted 15 July 2023
Available online 18 July 2023

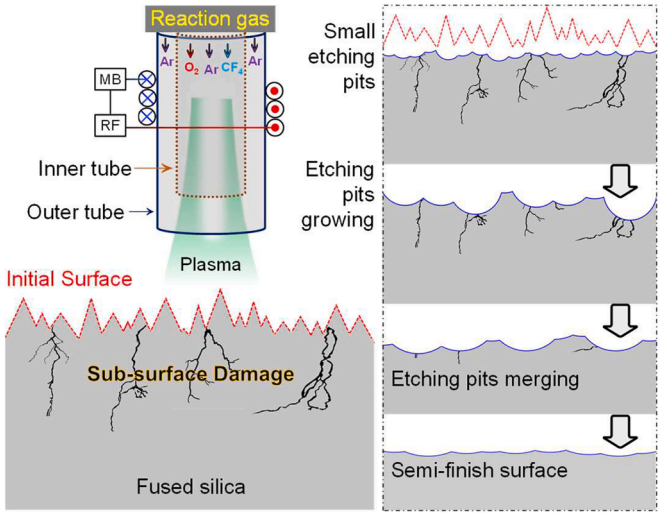

Fig. 1. Schematic of plasma-IEP mechanism.

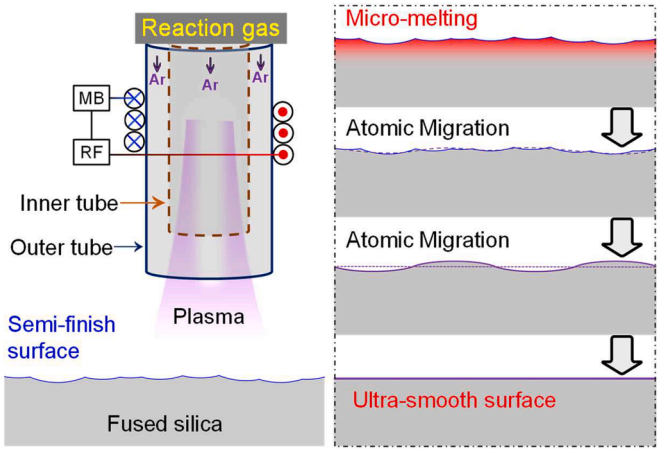

Fig. 2. Schematic of plasma-AMM mechanism.

material removal nature, plastic deformation or physical sputtering are involved in these techniques which makes it difficult to achieve a surface with less damage. In order to minimize damage, these processes often used the smallest possible material removal unit, which significantly limited their efficiency. In order to realize rapid transformation of surface roughness of fused silica from nanometer to atomic level, we have proposed the plasma-induced atom-migration manufacturing (plasma-AMM) technology based on ICP [16]. The atomic level roughness (*Sa* < 0.16 nm) of the fused silica surface was successfully obtained by cross-scale migration of atoms from the surface peaks to the valleys. The plasma-AMM was simple in operation and low in cost, so it can directly polish the fused silica sample under atmospheric conditions and was not limited by the sample size. Along with the increasing requirement on manufacturing accuracy, the atomic and close-to-atomic scale manufacturing (ACSM), in which materials are removed, transferred or added at the atomic level, has become the research focus in the field of advanced manufacturing recently [17–19]. The achievability of atomic level roughness of plasma-AMM makes it a promising approach for ACSM.

Considering the advantages of plasma-IEP and plasma-AMM processes, this study proposed a manufacturing method for ultra-smooth surface of fused silica with less damage that combined the two procedures. IEP and AMM were both based on atmosphere ICP, allowing flexible process switching. In addition, there was no mechanical or physical sputtering effect, so an ultra-smooth surface with less damage of fused silica could be achieved theoretically. This paper introduced the mechanisms and processes of plasma-IEP and plasma-AMM respectively, and then studied the remarkable results achieved by the hybrid combining process. Finally, the optical properties of fused silica surfaces manufactured by different processes were evaluated by laser induced damage threshold (LIDT) test.

2. Mechanisms of plasma-IEP and plasma-AMM

Plasma etching has been widely used in the manufacture of micro-electromechanical systems and microelectronic devices in combination with patterning processes like lithography. Plasma-IEP is based on the etching reaction between silicon-based substrates such as SiO_2 and the reactive radicals produced by dissociation of CF_4 as the reaction gas in ICP. As a nearly fully ionized plasma, ICP usually has a high temperature (up to 7000 K) and a high active particle density (10^{13}–10^{17} cm^{-3}) [20]. Thus, ICP is an ideal medium for efficient dry etching. The etching reaction can be described by Eq. (1):

$$SiO_2 + CF_4 \rightarrow SiF_4\uparrow + CO_2\uparrow \quad (1)$$

Fig. 1 shows the schematic semi-finishing mechanism of plasma-IEP process. At the beginning of etching, many etching pits randomly form on the surface of fused silica. The formation of the etching pits may be related to the distribution of damage or the competitive adsorption between F and O radicals on fused silica surface [21]. For amorphous fused silica, the evolution of the etching pits shows isotropic features with smooth inner surface and hemispherical contour. The subsurface damage of fused silica was reduced after etching for a certain duration. As the etching continues, the etching pits keep growing and gradually merge with each other. The height difference of overlapped peak sites and bottoms sites is also gradually reduced, so the etching process has an effective surface smoothing effect [22,23]. However, plasma-IEP always produces a boundary area between the etching pits, so the surface roughness cannot be reduced to sub-nanoscale [11], forming the new surface damage. Therefore, plasma-IEP can only be used as a semi-finishing method to obtain a smooth surface with nanoscale roughness.

Fig. 2 shows the schematic of plasma-AMM process. The key of plasma-AMM is the instantaneous energy input of ICP to the surface of fused silica, which induces the surface micro-melting effect. Thereafter, the atoms at protrusions migrate to valleys under the action of surface tension, thereby forming an ultra-smooth surface. The probable mechanism of plasma-AMM at the microscale is as follows. Under the action of plasma energy, the covalent bonds between Si and O atoms on the surface of fused silica are broken to form free atoms or clusters. There is only a weak van der Waals interaction between the free atoms and the surface atoms. The free atoms/clusters are weakly adsorbed on the surface and prone to migration. When the free atoms/clusters at protrusions are filled into valleys of the surface, the surface area of the fused silica decreased and so does the surface energy. According to the principle of energy minimization, the migration process continues until the surface reaches a stable low-energy state, corresponding to an ultra-smooth surface. Previous studies showed that atomic level smooth surface was obtained on fused silica based on ICP by the atomic migration effect [16,24].

3. Experimental setup and conditions

In this study, plasma-IEP and plasma-AMM used the same setup of numerical control triaxle platform with ICP excitation function. The device was mainly composed of a radio frequency (RF) power supply, a matcher, a copper inductor coil, a quartz torch tube, an alumina sample table and a three-axis CNC (computerized numerical control) motion system. The quartz torch was fixed at the center of the induction coil and consisted of two coaxial quartz tubes (outer diameter 20 mm, inner diameter 16 mm). Localized ICP irradiation was firstly conducted in

Table 1
Plasma-IEP and plasma-AMM parameters.

Parameters	Plasma-IEP	Plasma-AMM
Ignition gas (Ar)	1.5 slm	
Cooling gas (Ar)	18.0 slm	
CF_4	60 sccm	0
O_2	10 sccm	0
Frequency	27.12 MHz	
RF power	500 W	600–1400 W
Distance	15 cm	
Time	0.5–30 min	5 min

plasma-IEP, plasma-AMM and hybrid processes respectively for process optimization. Plasma-IEP was conducted to reduce the subsurface damage as revealed by wet etching in buffered hydrofluoric acid. Plasma-AMM was conducted to verify the surface smoothing capability. Then, scanning ICP irradiation was conducted in hybrid process on a lapped surface to realize less damage of the whole-surface and sub-nanometric smoothing.

In the IEP process, the inner tube supplied a small flow of ignition gas (Ar) and reaction gas (CF_4 and O_2), and the outer tube supplied a large flow of cooling gas (Ar) to prevent the quartz torch from melting at high temperatures and to stabilize the ICP plasma beam. The role of O_2 was to avoid the obstruction of the etching reaction after the fluorinated polymer deposited on the surface and to promote the dissociation of CF_4 [25,26]. Different from plasma-IEP, the inner and outer quartz torch tube only supplied high purity Ar in the plasma-AMM process. The flow and power parameters of the reaction gas used in plasma-IEP and plasma-AMM are shown in Table 1.

Fig. 3(a) shows the photos of plasma used in the IEP and AMM processes. The plasmas demonstrate different colors due to their different radical composition. The composition of free radicals in ICP was determined by an optical emission spectrometer (OES, Ocean Optics USB4000) with a wavelength resolution of 0.2 nm. The fiber optical probe was fixed 200 mm away from the center of the torch and recorded the spectral information of all collected data at a constant integration time of 60 ms. In plasma-IEP process, the power was constant at 500 W, corresponding to a surface average temperature of 802.7 °C over the beam region. In plasma-AMM process, RF power was increased from 600 to 1400 W. Thus, the surface temperature under different powers was measured, shown in Fig. 3(b). The result shows that the surface average temperature has an almost linear relationship with the power, which means the surface temperature can be controlled by power tuning.

In plasma-IEP process, CF_x (360–500 nm) and C_2 radicals generated intense peaks when Ar was used as the ignition gas and CF_4 and O_2 were used as the reaction gasses [27], as shown in Fig. 3(c). Due to the small difference between the peak positions of F and Ar, and the limited wavelength resolution of the spectrometer, the peak of fluorine radical couldn't be identified. However, the existence of CF_x and C_2 peaks could prove the dissociation of CF_4. This process inevitably produced F atoms, which were the main etching species in plasma-IEP [28]. In the process of plasma-AMM (RF power 1400 W), Ar was used as the ignition gas. Corresponding to the deexcitation of Ar atoms, only some strong Ar peaks (751.5 nm, 763.5 nm, 811.5 nm, 842.5 nm, etc.) were observed [29,30], as shown in Fig. 3(d).

The etching mechanism and process of plasma-IEP were studied using smooth fused silica samples with a size of 40 mm × 40 mm × 10 mm processed by mechanical polishing (MP) to clearly show the evolution of etching pits. In order to study the isotropic etching characteristics of fused silica during plasma-IEP, ICP static etching rather than scanning experiments was performed firstly. This method can avoid multiple etching of the same position, which makes it difficult to analyze the variation of etching pits. The polishing mechanism and process of plasma-AMM were studied by using ground fused silica samples with the same size, which can clearly illustrate the effect of fused silica surface smoothing.

Moreover, fused silica is widely used in high power laser systems as a common optical element material. Therefore, the optical properties of

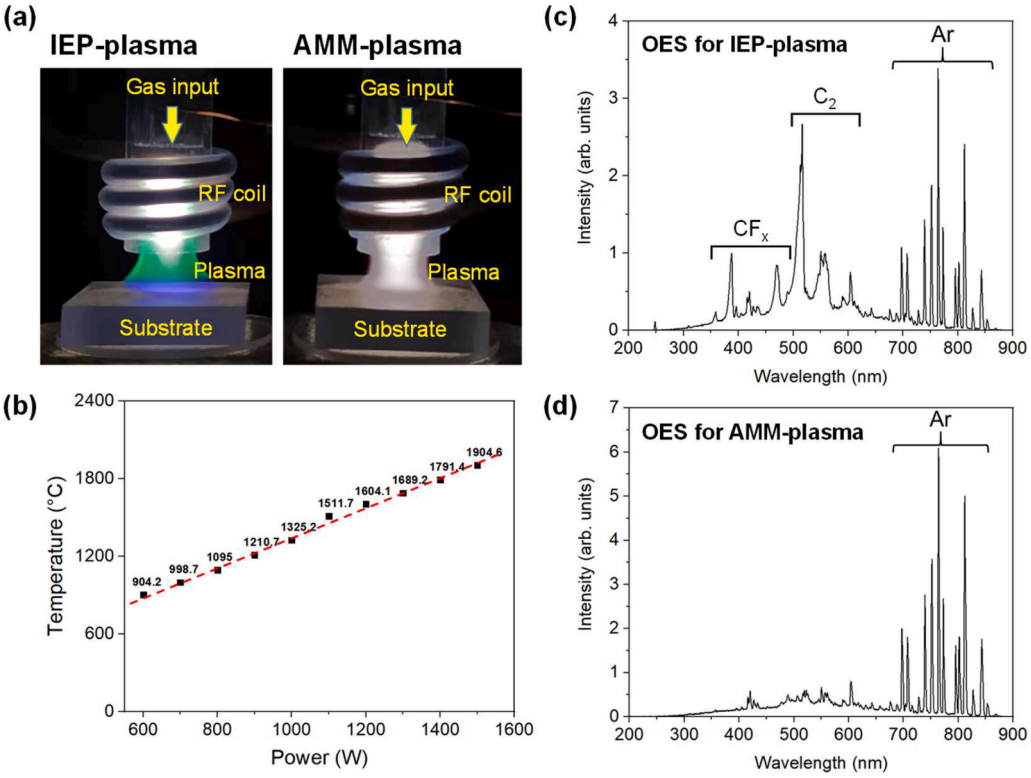

Fig. 3. (a) Photos of plasma used in plasma-IEP (left) and plasma-AMM (right); (b) Variation in surface temperature with RF power in plasma-AMM process; (c) OES spectrum of ICP torch in plasma-IEP process; (d) OES spectrum of ICP torch in plasma-AMM process (1400 W).

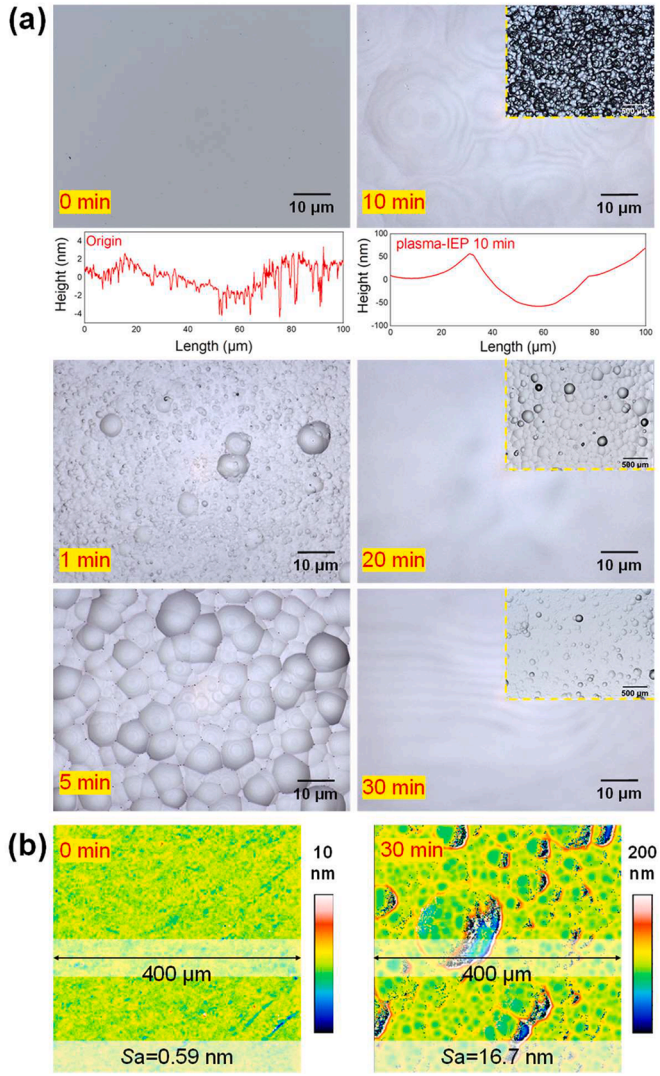

Fig. 4. (a) LSCM images and profiles of the fused silica surface processed by plasma-IEP with different durations. (Insets are LSCM images with low magnification); (b) SWLI images of the fused silica surface before and after plasma-IEP process.

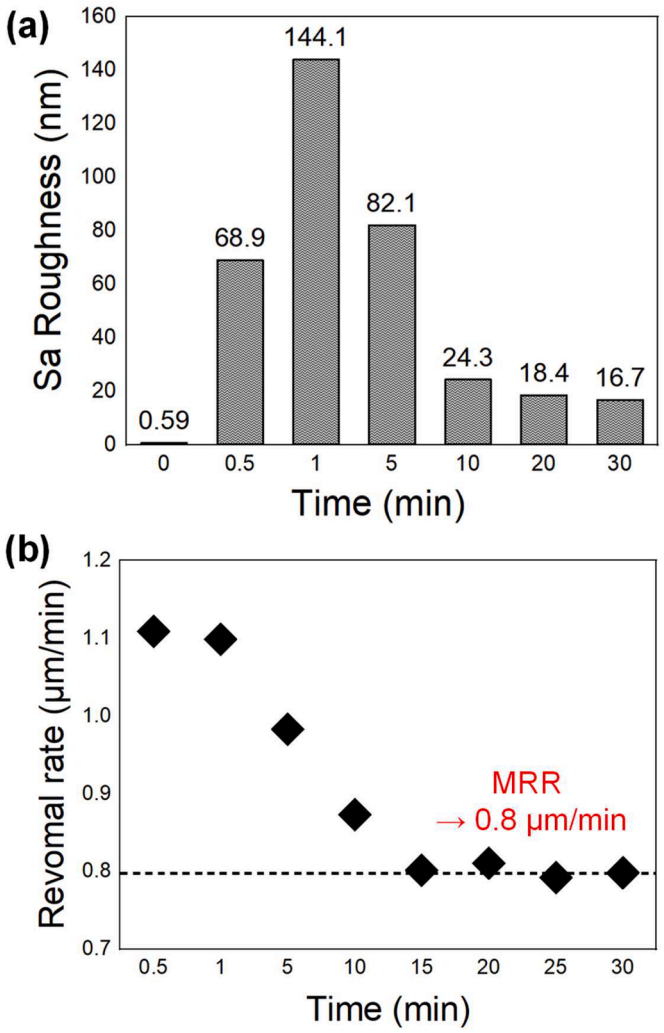

Fig. 5. (a) The evolution of the surface roughness (400 μm × 400 μm, by SWLI) of fused silica during plasma-IEP process; (b) The MRR of fused silica versus plasma-IEP time.

the surface of fused silica samples manufactured by various processes were evaluated by LIDT. In this study, the LIDT values of four different samples were tested at 515 nm and 1030 nm wavelengths respectively. The four fused silica samples were: #1 sample (initial sample, after MP), #2 sample (after plasma-AMM process), #3 sample (after plasma-IEP process), #4 sample (after IEP-AMM process). The test system consisted of a femtosecond laser, a three-dimensional motorized stage, a camera-based imaging module and a series of mirrors and lenses. The femtosecond laser (Pharos-10 W, Light Conversion) could generate output wavelengths of 1030 nm and 515 nm and enabled repetition rate adjustment. The pulse length of femtosecond laser was approximately 290 fs.

Firstly, the laser spot diameter and power at 515 nm and 1030 nm were measured by a spot analyzer (Newport, LBP2-HR-VIS2) and a power meter (Newport, 1919-R) respectively. After determining the minimum spot size focused by a lens (LBTEK, MCX10613) on the surface of samples, the LIDT values of the 4 samples were tested. During the test, the surface of each sample was irradiated with a single laser pulse on N lines with M points ($M \geq 10$) on each line. and the energy density for each line was fixed and decreased sequentially from top to bottom to find the LIDT values, which are the critical values of just damaging the surface of the samples. The point spacing and line spacing were set to 0.04 mm and 20 μm. The minimum spot radii of 515 nm and 1030 nm laser on the surface of the sample were about 8.73±0.09 μm and 13.61 ±0.31 μm respectively For the Gaussian beam, when the far-field conditions are satisfied, the radius of the spot is proportional to the propagation distance [31]. Thus, on the premise of meeting the far-field conditions, we measured the radii of spot size in different positions along the direction of propagation and recorded the propagation distances to calculate the minimum spot radii of 515 and 1030 nm by fitting linearly.

All samples were ultrasonically cleaned with high purity alcohol (99.5%), rinsed with ultra-pure water, and then dried with nitrogen (99.999%). The surface morphology of the sample was observed by a laser scanning confocal microscope (LSCM, Keyence VK-X1000), and the surface roughness was measured by a scanning white light interferometer (SWLI, Taylor Hobson M112–4449–02 CCI HD) and an atomic force microscope (AFM, Bruker Edge).

4. Plasma-IEP and plasma-AMM experimental results

Fig. 4(a) shows the surface morphology of fused silica processed by plasma-IEP with different durations. The initial surface was smooth and uniform, while the *Sa* roughness was 0.59 nm. A smooth surface was processed by reactive etching to better demonstrate the evolution of

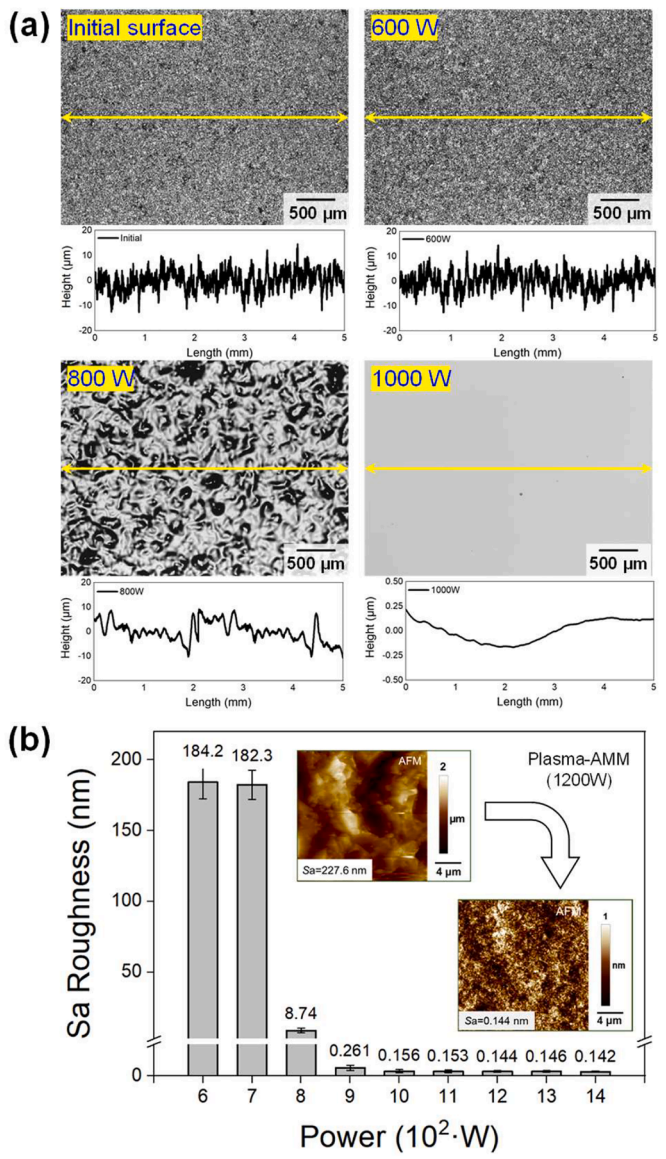

Fig. 6. (a) LSCM images and profiles of the fused silica surface after plasma-AMM process under different power levels; (b) Variation of the surface *Sa* roughness as a function of the RF power (20 μm × 20 μm, by AFM), the inset shows the AFM image of the initial surface and plasma-AMM processed surface at 1200 W.

etching pits morphology during plasma-IEP process. At the beginning of plasma-IEP process (1 min), small-sized etching pits were formed and the surface became rough. As plasma-IEP process continued, the etching pits grew up, overlapped and merged, with a smooth surface forming gradually. When plasma-IEP process time prolonged to 20 and 30 min, the sample presented a smooth surface in a scale of 100 μm. Fig. 4(a) also shows the profiles of the initial and plasma-IEP processed (10 min) surfaces. The initial surface has obvious high-frequency roughness. Although the etching boundaries generated by isotropic etching always existed on the surface in plasma-IEP process, the optical image and profile show that the inner surfaces of the etch pits were smooth.

However, it is worth noting that lots of pits can still be observed under a low-magnification view, as shown in the insets of Fig. 4(a). After 30 min of plasma-IEP, large-sized etch pits still existed on the surface. Fig. 4(b) shows the roughness images of the initial and plasma-IEP processed (30 min) surface. Compared with the initial smooth surface (*Sa* 0.59 nm), plasma-IEP processed surface was relatively rough (*Sa* 16.7 nm). As plasma etching of amorphous SiO_2 was an isotropic process [21], the subsurface damage was efficiently reduced whereas nanometer level roughness over a large scale was difficult to achieve.

Fig. 5(a) shows the evolution of the surface *Sa* roughness of fused silica processed by plasma-IEP with different durations, corresponding to the morphology change in Fig. 4(a). The *Sa* roughness of the fused silica surface increased to 144.1 nm rapidly (1 min). With the continuous growing up, overlapping and merging of the etching pits, the *Sa* roughness decreased gradually. After 20 min, the *Sa* roughness began to stabilize at the 10 nm level. As a semi-finishing process, the advantage of plasma-IEP is to remove material efficiently. The MRR of fused silica through plasma-IEP was investigated here, shown in Fig. 5(b). The MRR can be calculated by Eq. (2) [32]:

$$\mathrm{MRR} = \frac{\Delta m}{\rho \cdot \pi R^2 \cdot t} \tag{2}$$

where Δm represents the weight change of the sample before and after plasma-IEP; ρ is the density of fused silica, 2.203 $g \cdot cm^{-3}$; R is the radius of the ICP torch, 20 mm in this study; t is the IEP processing time. With the continuous processing of plasma-IEP, the etching reaction gradually stabilized and the MRR finally stabilized at 0.8 μm/min. Thus, plasma-IEP process was able to remove several microns of material from mechanical defects.

The achievable surface roughness after plasma-IEP was not satisfactory for optical applications. Thus, the finishing capability of plasma-AMM combined with plasma-IEP, was investigated. The principle of plasma-AMM is the instantaneous energy transfer from ICP to the surface, thereby inducing surface micro-melting. Therefore, RF power is the key factor controlling the plasma-AMM finishing effect.

Fig. 6(a) shows the LSCM images of initial surface and surface after 5 min plasma-AMM process at different RF powers. The initial grinding surface was very rough (*Sa* 227.6 nm) and contained obvious surface damage. When the power was 600 W, the ground surface morphology was almost unchanged. Because the heat transferred by ICP was not enough to completely melt the surface, the surface has a rippled appearance at 800 W. When the power reached 1000 W, an ultra-smooth surface was formed. Fig. 6(a) also shows the surface profiles at different powers. The initial rough profile became smoother gradually after plasma-AMM as the power increased over 800 W. However, it can also be found that there is an obvious millimeter-scale low spatial frequency fluctuation on the surface processed by 1400 W ICP which is considered caused by thermal expansion. Fig. 6(b) shows the variation of the *Sa* roughness with the RF power, measured by the AFM (20 μm scale). When the power was lower than 700 W, the *Sa* roughness was still on 100 nm level. When the power increased to 800 W, the *Sa* roughness decreased to nanoscale (8.74 nm). Moreover, when the power further increased to 900 W, the *Sa* roughness decreased to atomic level (0.26 nm). When the power exceeded 1000 W, the *Sa* roughness can be stabilized at about 0.15 nm, corresponding to an ultra-smooth surface with atomic level precision.

It has been proved that atomic level smooth surface can be realized by plasma-AMM. However, the subsurface damage should be verified. Lorenz Livermore National Laboratory used HF acid etching to detect and enhance the LIDT of polished fused silica surface [33], which can expose defects masked by the re-deposited layer. The chemical reaction of fused silica in HF acid can be expressed as Eq. (3) [34]:

$$SiO_{2\,(solid)} + 3HF^{2-}{}_{(aq)} + H^{+}{}_{(aq)} \rightarrow SiF_6^{2-}{}_{(aq)} + 2H_2O_{(aq)} \tag{3}$$

HF cannot be fully ionized in water, so the solution contains H^+, F^-, HF^{2-} ions, undissolved HF molecules, and $(HF)_n$ clusters were formed by hydrogen bonding, such as $(HF)_2$. To realize a stable etching rate, NH_4F solution was added to HF solution, which was called buffered oxide etch (BOE) [35] solution. Therefore, dip in BOE solution (5% HF and 10% NH_4F mass fraction, 17 °C) was used as a visual approach to detect the subsurface damage of fused silica.

The initial, plasma-IEP processed and plasma-AMM processed

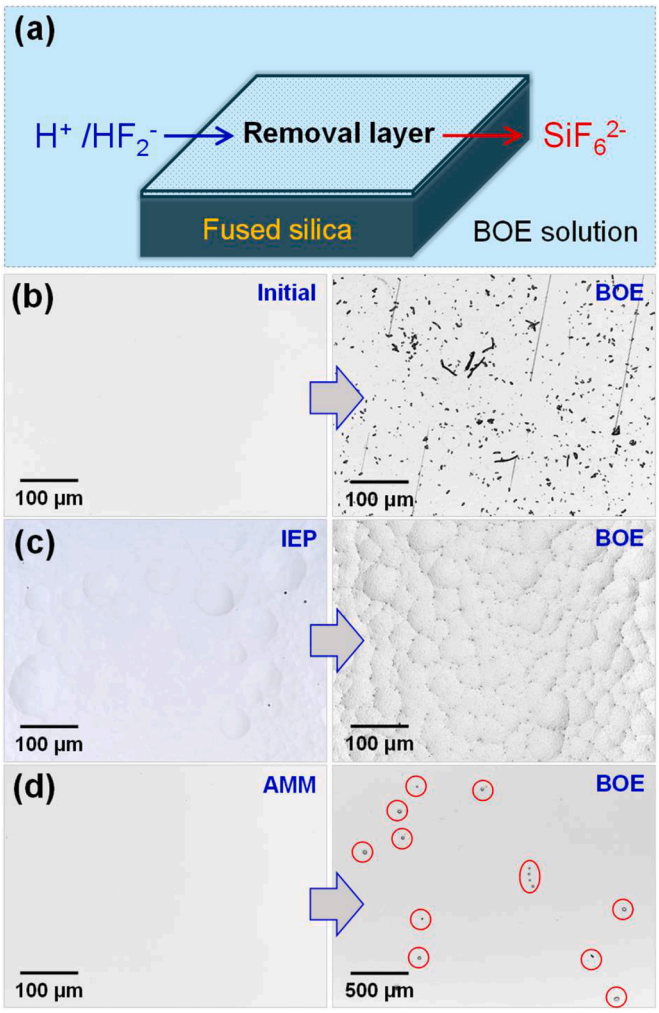

Fig. 7. (a) Schematic of BOE solution etching for fused silica; Surface morphology of fused silica in BOE solution for 10 min: (b) Initial surface (after MP); (c) Plasma-IEP 20 min; (d) Plasma-AMM (1200 W).

samples were selected as the etching objects of the BOE solution. The etching reaction between BOE solution and fused silica is illustrated in Fig. 7(a). The LSCM images of the initial and BOE-processed surfaces are shown in Fig. 7(b). A large number of defects with different sizes and morphology were exposed on the surface after BOE, which indicated that there was a large amount of subsurface damage on the initial surface. The LSCM images of the plasma-IEP processed and subsequently BOE processed surfaces are shown in Fig. 7(c). No new defect was exposed on the surface after BOE, although the pit contours were sharper. It indicated that plasma-IEP process reduced the subsurface damage hidden beneath the initial sample surface.

The LSCM images of the surface processed by plasma-AMM and subsequent BOE are shown in Fig. 7(d). The surface after plasma-AMM process was smooth and bright. After dipping in BOE solution, the surface still exposed a small amount of damage morphology, which also meant that plasma-AMM cannot completely recovery the subsurface defects of fused silica. When plasma-AMM was applied to a severely damaged surface, the surface would be quickly smoothed by rapid migration of top surface material. However, this will hinder the recovery of the thick damage beneath [16]. Therefore, once the plasma-AMM processed surface was further processed by BOE, the hindered subsurface damage was exposed. This also proved the necessity to combine plasma-IEP with plasma-AMM rather than to use one single process.

5. IEP-AMM hybrid manufacturing process

Based on the above research, we proposed the IEP-AMM hybrid manufacturing process, in which plasma-IEP played the role to efficiently reduce the subsurface damage layer while plasma-AMM was utilized to smooth the surface to atomic level. The lapped fused silica samples (P600 sandpaper) with a size of 40 mm × 40 mm × 10 mm were used to study the effect of IEP-AMM hybrid manufacturing.

As shown in Fig. 8(a), there was a large number of scratches and indentation damages on the lapped surface. The *Sa* roughness of the lapped surface was on the order of 97.1 nm, with the maximum scratch depth over 500 nm. Guided by the previous research, plasma-IEP was used for 20 min etching, and then plasma-AMM was used at 1400 W power. Finally, the fused silica sample obtained by hybrid manufacturing was dipped in BOE solution (10 min) for acid etching to expose the subsurface damage if any. Fig. 8(b) shows the surface morphology after the IEP process. Uniform-etching pits were formed on the surface without scratch damage.

The SWLI image shows that the *Sa* roughness was reduced from 97.1 nm to 31.3 nm. Fig. 8(c) shows the surface morphology after IEP-AMM hybrid manufacturing process. The etching pit morphology formed by plasma-IEP process transformed into an ultra-smooth surface after plasma-AMM process, with the *Sa* roughness reduced to 0.17 nm, which

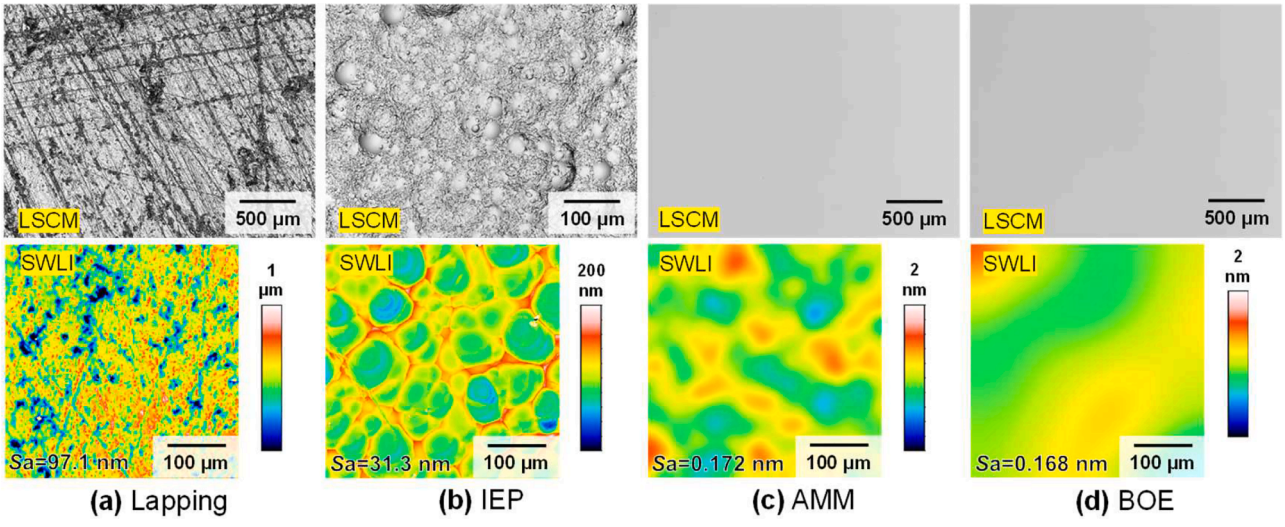

Fig. 8. Surface morphology (LSCM) and *Sa* roughness (SWLI) of fused silica: (a) Lapped; (b) After plasma-IEP; (c) After IEP-AMM; (d) After etching by BOE.

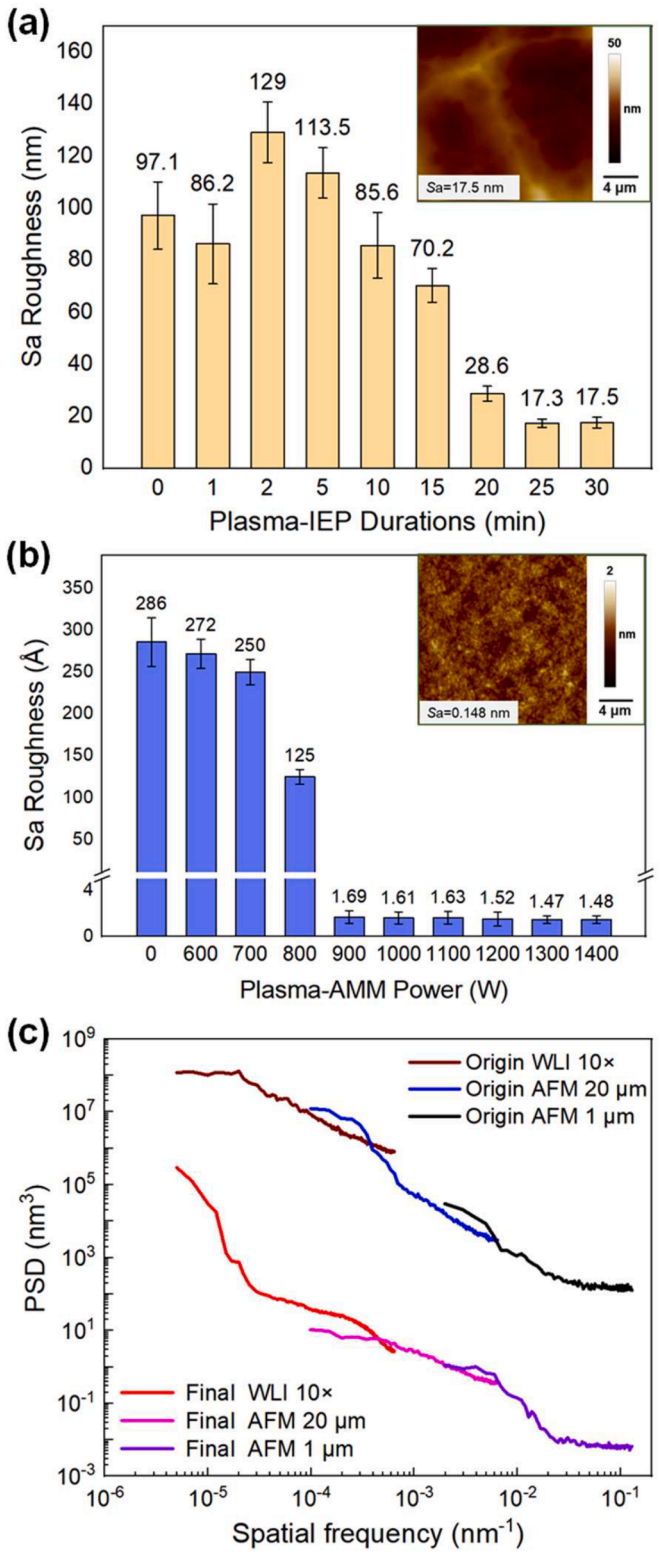

Fig. 9. (a) Surface roughness (AFM) with different durations of IEP (Inset shows an AFM image after IEP for 30 min); (b) Surface roughness (AFM) under different powers of plasma-AMM (Inset shows an AFM image after plasma-AMM at 1400 W); (c) PSD curves of fused silica surface before and after IEP-AMM hybrid process.

is comparable with the common optical manufacturing techniques like MRF process (Ra 0.165 nm [36]), IBF process (RMS 0.559 nm [37]) and laser finishing process (RMS 0.156 nm [38]). Therefore, IEP-AMM hybrid process can be regarded as an efficient polishing process to achieve atomic level roughness on fused silica surface.

In order to further explore the subsurface damage layer, BOE etching of the hybrid-processed surface was conducted. As seen in Fig. 8(d), the LSCM and SWLI images illustrated the absence of subsurface damage. Therefore, IEP-AMM hybrid manufacturing can be regarded as a manufacturing process with less damage of fused silica surface. This is also the most valuable advantage of the hybrid plasma process compared with conventional optical manufacturing processes like CCOS, MRF and IBF. Owing to the abrasion-based removal mechanism, CCOS and MRF will inevitably introduce subsurface damage [39]. For IBF process, the bombardment of ions also causes processing deterioration layer and residual stress on the surface [40,41]. However, some mid-spatial-frequency (MSF) errors (waviness) could be observed on the IEP-AMM-processed surface and the BOE-processed surface. The former is considered to be mainly caused by the residual etching pits of IEP, while the latter is supposed to be caused by the inconsistency etching depth of BOE.

In order to better optimize IEP-AMM hybrid process, the influence of key parameters in the two processes were studied respectively. In the IEP process, the etching duration determined the elimination degree of the subsurface damaged layer and the surface roughness. Fig. 9(a) shows the variation of the *Sa* roughness of fused silica at different IEP durations. For the lapped fused silica surface, plasma-IEP reduced the *Sa* roughness to 28.6 nm after 20 min with a removal depth of 16 μm. The etching processes by BOE have been performed on the samples processed by IEP with different durations and the subsurface damage layer of sample was efficiently reduced after 20 min of IEP. Therefore, 20 min was used to realize semi-finishing in the IEP process, considering the efficiency and reduce of subsurface damage.

The polishing effect of plasma-AMM was determined by the intensity of energy feeding, which could be tuned by the RF power. For the IEP-processed fused silica (20 min), subsequent plasma-AMM processes (5 min) were performed based on different RF powers. Fig. 9(b) shows the *Sa* roughness after plasma-AMM versus the power. When the power was lower than 700 W, the *Sa* roughness was still on 20 nm level; when the power reached 800 W, the *Sa* roughness was reduced to 12.5 nm; when the power exceeded 900 W, the *Sa* roughness was reduced to atomic level; when the power reached 1200 W, the *Sa* roughness was stabilized at about 0.15 nm. Therefore, the optimized processing parameters were plasma-IEP for 20 min and plasma-AMM at 1300 W, which efficiently transformed the lapped surface into a damage-reduced and ultra-smooth surface with *Sa* roughness below 0.15 nm.

Furthermore, the spatial frequency information of the surface was analyzed to investigate the possibility of removing different spatial frequency errors by the IEP-AMM hybrid manufacturing process. The surface morphology data used for calculating the power spectral density (PSD) were measured using the AFM with a probing area of 1×1 μm^2 and 20×20 μm^2, and the WLI with a measuring area of 400×400 μm^2. As shown in Fig. 9(c), the proposed IEP-AMM hybrid approach was effective for decreasing the surface residual error across the whole measured spatial frequency range. Similarly, CO_2 laser polishing formed obvious waviness errors on the surface of fused silica due to the thermal effect [42,43]. Thus, a figuring process is required to improve the form accuracy of the surface processed by IEP-AMM hybrid process.

To demonstrate the applicability of IEP-AMM hybrid process for large-size substrates, whole surface finishing by scanning on a 40×40 mm^2 fused silica substrate was carried out. The photo of the initial ground sample is shown in Fig. 10(a) and the scanning path is shown in Fig. 10(b). The scanning paths for plasma-IEP and plasma-AMM were the same. In plasma-IEP process, the scanning speed was 3.5 mm/min and the processing time was 40 min. In plasma-AMM process, the scanning speed was 10 mm/min and the power was 1300 W. After IEP-

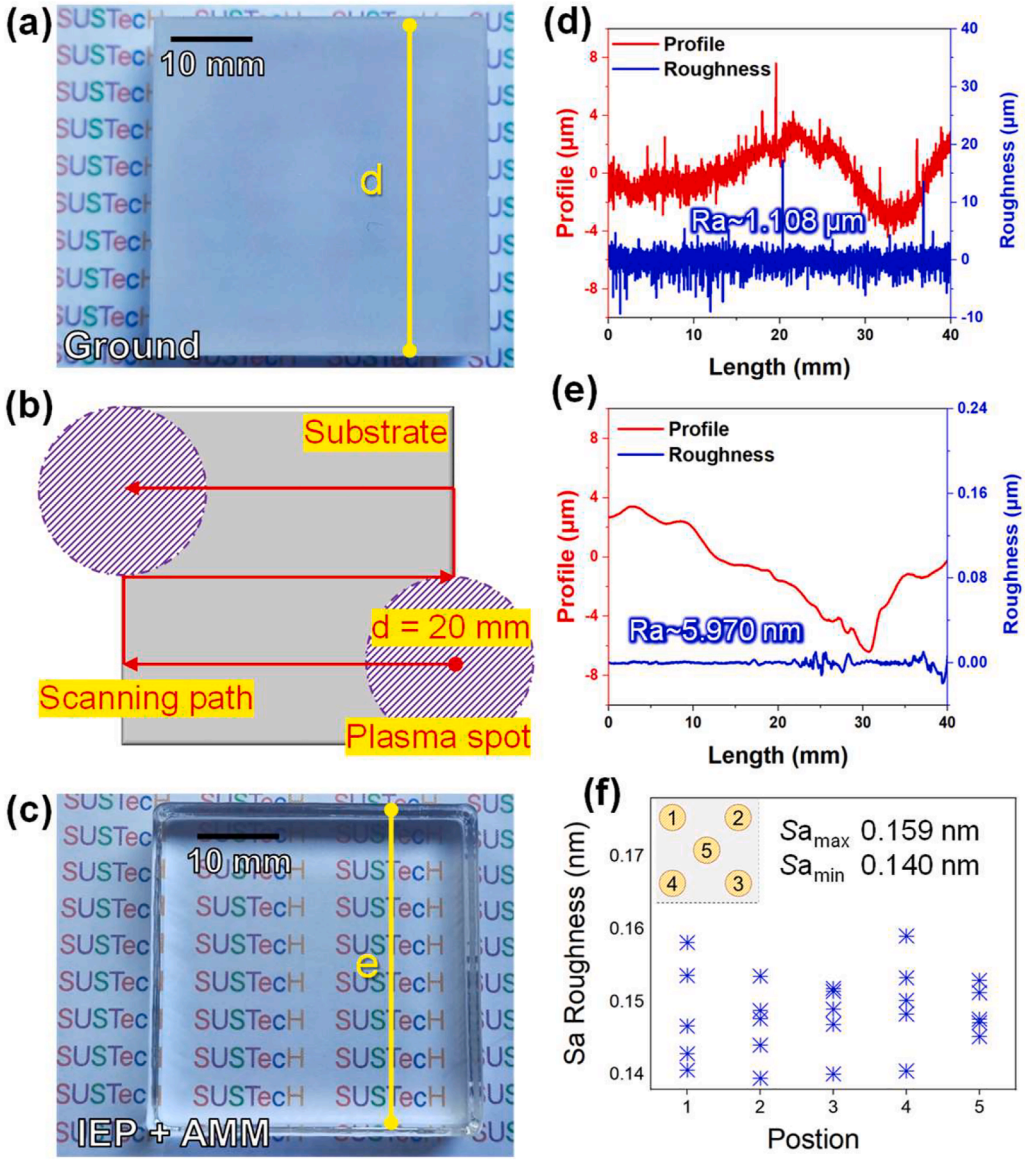

Fig. 10. (a) Photo of the ground fused silica sample; (b) ICP scanning path; (c) Photo of the fused silica sample after the IEP-AMM hybrid process; The profile and roughness of cross section on initial surface (d) and IEP-AMM processed surface (e); (f) The *Sa* roughness (20 μm × 20 μm, by AFM) value after IEP-AMM process (Inset shows the point distribution).

AMM hybrid process, a transparent fused silica sample with mirror surface was obtained as shown in Fig. 10(c). Fig. 10(d) and (e) shows the profile and roughness of initial surface and IEP-AMM hybrid processed surface. After IEP-AMM hybrid process, the *Ra* roughness decreased from 1.108 μm to 5.97 nm. However, it could be found that there is an obvious millimeter-scale low-spatial-frequency fluctuation on the surface. The *Sa* roughness was very constant varying from 0.140 nm to 0.159 nm, as shown in Fig. 10(f). For the fused silica sample after hybrid process, five points were randomly selected in region 1–5 to measure the roughness, as shown in inset.

The LIDT values of the four samples tested with 515 nm and 1030 nm lasers are marked with yellow numbers in Fig. 11(a) and (b). Fig. 11(c) gives the LIDT values of the samples at the two wavelengths. In the test results for 515 nm, the LIDT values of #2 sample and #4 sample increased from 2.2 J/cm^2 to 2.5 J/cm^2 and 2.8 J/cm^2, respectively. In the test results for 1030 nm wavelength, the LIDT value of #2 sample and #4 sample increased from 2.9 J/cm^2 to 3.4 J/cm^2 and 3.3 J/cm^2, respectively. Although the LIDT value of #3 sample increased to 3.9 J/cm^2, the surface of #3 sample is not very flat, which may cause laser defocusing during the LIDT test, so the measured LIDT value may not be very representative. It is expected that the #4 LIDT result would show a significant increase compared to the samples with only plasma-AMM, but there is in fact a small decrease compared to the result for #2 sample for 1030 nm, which needs further study.

For LIDT, in previous relevant studies, damage in the bulk of fused silica induced by femtosecond to nanosecond laser pulse has been investigated experimentally and theoretically. With the development of technology, the femtosecond laser is widely used in optics and it can damage fused silica through excitation of an electron-ion plasma triggered by avalanche [44], which may be different from the mechanism of damaging induced by nanosecond laser with collisional and multi-photon ionization, and plasma formation [45]. In addition, as shown in the Fig. 11(c), the LIDT values for 1030 nm are higher than those for 515 nm for 4 samples, which are consistent with the results in the Reference [46].

In summary, the plasma-based IEP-AMM hybrid manufacturing process not only realized an ultra-smooth surface with less damage manufacturing of fused silica, but also increased the LIDT, which

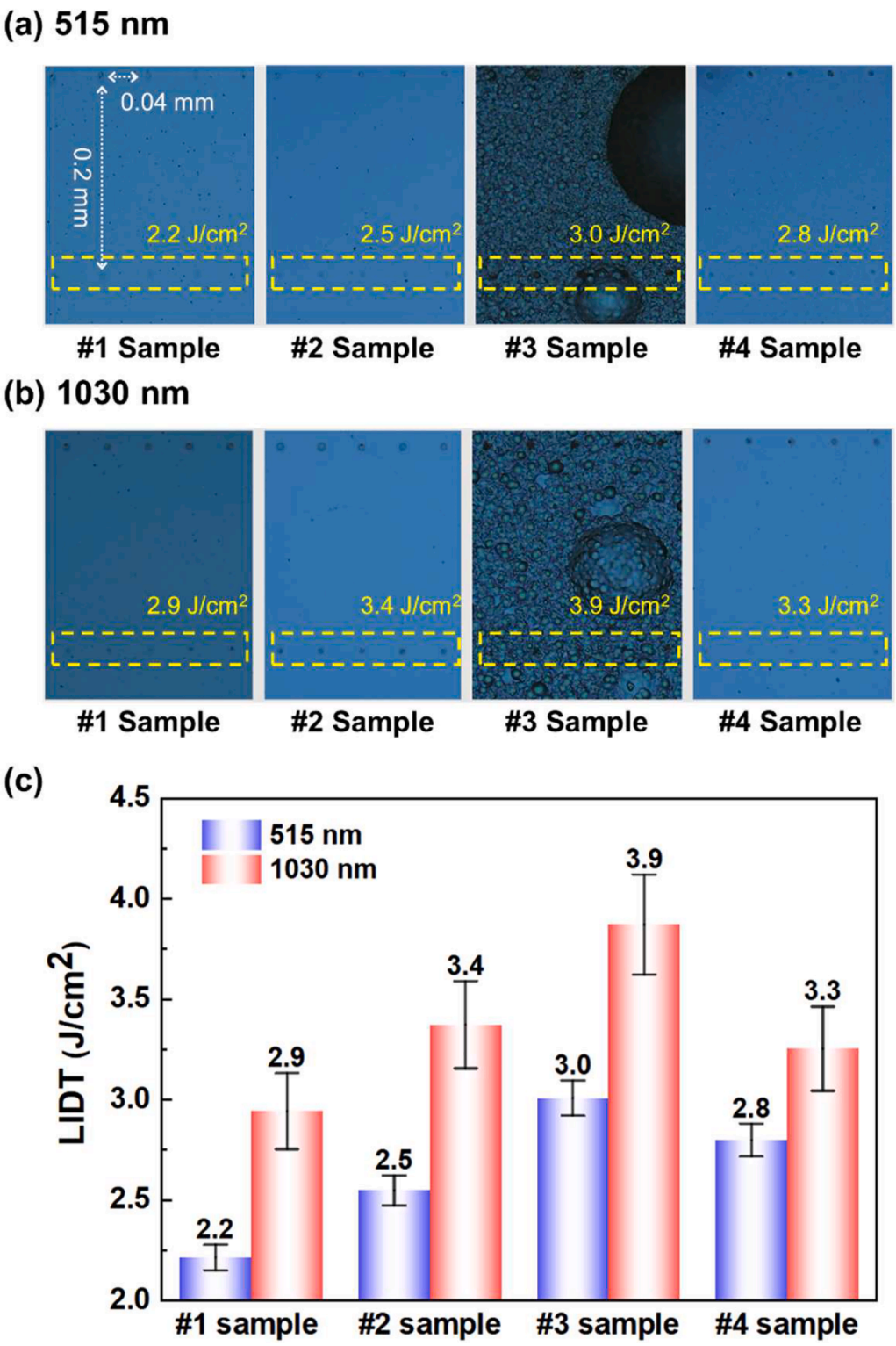

Fig. 11. The 20 × optical images of damaged points on the sample for (a) 515 nm and (b) 1030 nm femtosecond laser (the LIDT values are marked with yellow numbers): #1 sample (Initial, MP), # 2 sample (plasma-AMM processed), # 3 sample (plasma-IEP processed) and # 4 sample (IEP-AMM processed); (c) LIDT values of different samples for 515 nm and 1030 nm femtosecond laser.

showed that the fused silica could be better applied in high-power laser systems. The LIDT test method we used only provided a better evaluation of high defect density while the level of defect density in the sample was unknown. So, it is necessary to conduct systematic LIDT test in the further to obtain more accurate and specific values of LIDT indeed.

6. Conclusion

In this paper, a hybrid manufacturing process combining plasma-IEP and plasma-AMM was proposed for an atomic level smooth surface with less damage of fused silica. The following conclusions can be drawn from this study:

- Plasma-IEP, as a dry etching process, has the advantages of highly efficiency of reducing damage and reaching semi-finishing roughness on the order of 10 nm. Plasma-AMM, as a net manufacturing process, is superior in atomic-level roughness achievement.
- The combination process of plasma-IEP and plasma-AMM has been proved useful to realize ultra-smooth surface with less damage of fused silica. An atomic level smooth surface with *Sa* roughness < 0.2 nm has been achieved. The reduction of subsurface damage was confirmed by etching with BOE. The capability to process large size substrates by plasma scanning was demonstrated.
- The surface optical quality was confirmed by LIDT with femtosecond laser. After the plasma-based IEP-AMM hybrid process, the LIDT values of the fused silica surface increased from 2.2 J/cm^2 to 2.8 J/cm^2 for 515 nm and from 2.9 J/cm^2 to 3.3 J/cm^2 for 1030 nm, which demonstrated its potential applications in high power laser systems.

This paper showed that the developed IEP-plasma-AMM hybrid process can be an effective approach of ACSM, which has the potential to be further extended for atomically smooth surfaces with millimeter scale. This approach will open up new possibilities for cutting-edge optical research and applications which have stringent requirements for atomically smooth surface with less damage.

CRediT authorship contribution statement

Shaoxiang Liang: Data curation, Conceptualization, Methodology, Writing – original draft. **Yi He:** Data curation, Investigation. **Pengbo Ding:** Data curation, Investigation. **Chunjin Wang:** Writing – review & editing. **Liang Guo:** Methodology, Supervision, Writing – review & editing. **Hui Deng:** Conceptualization, Methodology, Funding acquisition, Supervision, Writing – review & editing.

Declaration of Competing Interest

The authors declare that they have no known competing financial interests or personal relationships that could have appeared to influence the work reported in this paper.

Data availability

Data will be made available on request.

Acknowledgment

This project is supported by the Natural Science Foundation of Guangdong Province (2023A1515011461) and the Science, Technology and Innovation Commission of Shenzhen Municipality (JCYJ20220818100412027, JCYJ20210324120402007). The author acknowledges the assistance of SUSTech Core Research Facilities.

References

[1] E.I. Moses, The national ignition facility (NIF): a path to fusion energy, Energy Convers. Manag. 49 (2008) 1795–1802.
[2] J.H. Campbell, R.A. Hawley-Fedder, C.J. Stolz, J.A. Menapace, M.R. Borden, P. K. Whitman, J. Yu, M.J. Runkel, M.O. Riley, M.D. Feit, NIF optical materials and fabrication technologies: an overview. The National Ignition Facility, International Society For Optics and Photonics, Optical Engineering at the Lawrence Livermore National Laboratory II, 2004, pp. 84–101.
[3] C.J. Stolz, Status of NIF mirror technologies for completion of the NIF facility. Advances in Optical Thin Films III, SPIE, 2008, pp. 420–430.
[4] W. Ulrich, H.J. Rostalski, R.M. Hudyma, Development of dioptric projection lenses for deep ultraviolet lithography at Carl Zeiss, J. Micro/Nanolithogr. 3 (2004) 87–96. MEMS MOEMS.
[5] M. Rothschild, T.M. Bloomstein, J.E. Curtin, D.K. Downs, C.V. Peski, 157 nm: deepest deep-ultraviolet yet, Sci. Technol. B Microelectron. Nanom. Struct. Process. Meas. Phenom. 17 (1999) 3262–3266.
[6] M. Serhatlioglu, B. Ortaç, C. Elbuken, N. Biyikli, M.E. Solmaz, CO2 laser polishing of microfluidic channels fabricated by femtosecond laser assisted carving, J. Micromech. Microeng. 26 (2016), 115011.
[7] C. Kunz, S. Engel, F.A. Müller, S. Gräf, Large-area fabrication of laser-induced periodic surface structures on fused silica using thin gold layers, Nanomaterials 10 (2020) 1187.
[8] N. Taniguchi, Current status in, and future trends of, ultraprecision machining and ultrafine materials processing, CIRP Ann. 32 (1983) 573–582.
[9] Y. Li, N. Zheng, H. Li, J. Hou, X. Lei, X. Chen, Z. Yuan, Z. Guo, J. Wang, Y. Guo, Morphology and distribution of subsurface damage in optical fused silica parts: bound-abrasive grinding, Appl. Surf. Sci. 257 (2011) 2066–2073.
[10] T. Suratwala, L. Wong, P. Miller, M. Feit, J. Menapace, R. Steele, P. Davis, D. Walmer, Sub-surface mechanical damage distributions during grinding of fused silica, J Non Cryst Solids 352 (2006) 5601–5617.
[11] R. Li, Y. Zhang, Y. Zhang, W. Liu, Y. Li, H. Deng, Plasma-based isotropic etching polishing of synthetic quartz, J. Manuf. Process 60 (2020) 447–456.
[12] R.A. Jones, Optimization of computer controlled polishing, Appl. Opt. 16 (1977) 218–224.
[13] M. Kumar, A. Kumar, A. Alok, M. Das, Magnetorheological method applied to optics polishing: a review, in: Proceedings of the IOP Conference Series: Materials Science and Engineering, IOP Publishing, 2020, 012012.
[14] T. Arnold, G. Böhm, R. Fechner, J. Meister, A. Nickel, F. Frost, T. Hänsel, A. Schindler, Ultra-precision surface finishing by ion beam and plasma jet techniques—Status and outlook, Nucl. Instrum. Methods. Phys. Res. A 616 (2010) 147–156.
[15] B. Lin, K.L. Li, Z.C. Cao, T. Huang, Modeling of pad surface topography and material removal characteristics for computer-controlled optical surfacing process, J. Mater. Process. Technol. 265 (2019) 210–218.
[16] S. Liang, L. Zhang, H. Deng, Theoretical and experimental study on plasma-induced atom-migration manufacturing (PAMM) of glass, Appl. Surf. Sci. 599 (2022), 153976.
[17] F. Fang, The three paradigms of manufacturing advancement, J. Manuf. Syst. 63 (2022) 504–505.
[18] F. Fang, Atomic and close-to-atomic scale manufacturing: perspectives and measures, Int. J. Extreme Manuf. 2 (2020), 030201.
[19] N. Yu, S. Reid, R. Cheung, V. Koutsos, Foreword to the special issue on nanomanufacturing and atomic & close-to-atomic scale manufacturing (ACSM), Nanomanufacturing Metrol. 5 (2022) 189–190.
[20] T. Ichiki, R. Taura, Y. Horiike, Localized and ultrahigh-rate etching of silicon wafers using atmospheric-pressure microplasma jets, J. Appl. Phys. 95 (2004) 35–39.
[21] B. Wu, Y. Zhang, R. Yi, H. Deng, Tuning the plasma etching mode for the atomic-scale smoothing of single-crystal silicon, J. Phys. Chem. Lett. 13 (2022) 8580–8585.
[22] R. Yi, Y. Zhang, X. Zhang, F. Fang, H. Deng, A generic approach of polishing metals via isotropic electrochemical etching, Int. J. Mach. Tools Manuf. 150 (2020), 103517.
[23] R. Yi, Z. Zhan, H. Deng, Isotropic tuning of electrochemical etching for the nanometric finishing of metals, Nanomanufacturing Metrol. 5 (2022) 283–296.
[24] R. Li, Y. Li, H. Deng, Plasma-induced atom migration manufacturing of fused silica, Precis. Eng. 76 (2022) 305–313.
[25] Y. Zhang, R. Li, Y. Zhang, D. Liu, H. Deng, Indiscriminate revelation of dislocations in single crystal SiC by inductively coupled plasma etching, J. Eur. Ceram. Soc. 39 (2019) 2831–2838.
[26] C. Mogab, A. Adams, D. Flamm, Plasma etching of Si and SiO2—the effect of oxygen additions to CF4 plasmas, J. Appl. Phys. 49 (1978) 3796–3803.
[27] R. Wang, C. Zhang, X. Liu, Q. Xie, P. Yan, T. Shao, Microsecond pulse driven Ar/CF4 plasma jet for polymethylmethacrylate surface modification at atmospheric pressure, Appl. Surf. Sci. 328 (2015) 509–515.
[28] S. Zimmermann, N. Ahner, F. Blaschta, M. Schaller, H. Rülke, S. Schulz, T. Gessner, Analysis of the impact of different additives during etch processes of dense and porous low-k with OES and QMS, Microelectron. Eng. 87 (2010) 337–342.
[29] A. Sarani, A.Y. Nikiforov, C. Leys, Atmospheric pressure plasma jet in Ar and Ar/H 2 O mixtures: optical emission spectroscopy and temperature measurements, Phys. Plasmas 17 (2010), 063504.
[30] M. Song, Y. Lee, T. Chung, Characterization of an inductively coupled nitrogen-argon plasma by Langmuir probe combined with optical emission spectroscopy, Phys. Plasmas 18 (2011), 023504.
[31] F.L. Pedrotti, L.M. Pedrotti, L.S. Pedrotti, Introduction to Optics, Cambridge University Press, 2017.
[32] Q. Luo, J. Lu, X. Xu, F. Jiang, Removal mechanism of sapphire substrates (0001, $11\bar{2}0$ and $10\bar{1}0$) in mechanical planarization machining, Ceram. Int. 43 (2017) 16178–16184.
[33] P. Bouchut, P. Garrec, C. Pelle, Wet etching for the mitigation of laser damage growth in fused silica. Laser-Induced Damage in Optical Materials: 2002 and 7th International Workshop On Laser Beam and Optics Characterization, SPIE, 2003, pp. 103–111.
[34] L. Wong, T. Suratwala, M. Feit, P. Miller, R. Steele, The effect of HF/NH4F etching on the morphology of surface fractures on fused silica, J. Non Cryst Solids 355 (2009) 797–810.
[35] H. Proksche, G. Nagorsen, D. Ross, The Influence of NH 4 F on the etch rates of undoped SiO2 in buffered oxide etch, J. Electrochem. Soc. 139 (1992) 521.
[36] M.K. Gupta, D. Dinakar, I.M. Chhabra, S. Jha, B.S. Madireddy, Experimental investigation and machine parameter optimization for nano finishing of fused silica using magnetorheological finishing process, Optik 226 (2021), 165908. Stuttg.

[37] J. Ji, W. Fan, W. Gao, C. Wang, Y. Zhang, M. Xu, F. Ji, Investigation of roughness evolution of ion sputtered fused silica surface, Appl. Opt. 58 (2019) 5388–5396.
[38] T. He, C. Wei, Z. Jiang, Y. Zhao, J. Shao, Super-smooth surface demonstration and the physical mechanism of CO 2 laser polishing of fused silica, Opt. Lett. 43 (2018) 5777–5780.
[39] Z. Wu, G. Li, Y. Jia, Q. Lv, S. Deng, Y. Jin, Investigation on morphology and chemistry of the Beilby layer on polished fused silica, Ceram. Int. 49 (2023) 17116–17122.
[40] M. Xu, F. Shi, L. Zhou, Y. Dai, X. Peng, W. Liao, Investigation of laser-induced damage threshold improvement mechanism during ion beam sputtering of fused silica, Opt. Express 25 (2017) 29260–29271.
[41] N. Chkhalo, S. Churin, A. Pestov, N. Salashchenko, Y.A. Vainer, M. Zorina, Roughness measurement and ion-beam polishing of super-smooth optical surfaces of fused quartz and optical ceramics, Opt. Express 22 (2014) 20094–20106.
[42] A. Temmler, C.B. Weingarten, B. Schober, E. Uluz, Investigation on laser beam figuring of fused silica using microsecond pulsed CO2 laser radiation, Appl. Surf. Sci. 555 (2021), 149609.
[43] L. Zhao, J. Cheng, M. Chen, X. Yuan, W. Liao, Q. Liu, H. Yang, H. Wang, Formation mechanism of a smooth, defect-free surface of fused silica optics using rapid CO2 laser polishing, Int. J. Extreme Manuf. 1 (2019), 035001.
[44] A. Couairon, L. Sudrie, M. Franco, B. Prade, A. Mysyrowicz, Filamentation and damage in fused silica induced by tightly focused femtosecond laser pulses, Phys. Rev. B 71 (2005), 125435.
[45] B. Stuart, M. Feit, A. Rubenchik, B. Shore, M. Perry, Laser-induced damage in dielectrics with nanosecond to subpicosecond pulses, Phys. Rev. Lett. 74 (1995) 2248.
[46] D.B. Douti, L. Gallais, M. Commandré, Laser-induced damage of optical thin films submitted to 343, 515, and 1030nm multiple subpicosecond pulses, Opt. Eng. 53 (2014), 122509, 122509.